

Bi-Temporal Semantic Reasoning for the Semantic Change Detection of HR Remote Sensing Images[★]

Ding Lei^a, Guo Haitao^{b,*}, Liu Sicong^c, Mou Lichao^d, Zhang Jing^a and Lorenzo Bruzzone^{a,**}

^aUniversity of Trento, Via Sommarive 5, I-38123, Trento, Italy.

^bStrategic Support Force Information Engineering University, Zhengzhou 450001, P.R. China.

^cCollege of Surveying and Geoinformatics, Tongji University, No.1239 Siping Road, Shanghai, P.R. China.

^dRemote Sensing Technology Institute, German Aerospace Center, and Signal Processing in Earth Observation, Technical University of Munich, Germany

ARTICLE INFO

Keywords:

Remote Sensing
Convolutional Neural Network
Semantic Segmentation
Change Detection
Semantic Change Detection

ABSTRACT

Semantic change detection (SCD) extends the change detection (CD) task to provide not only the change locations but also the detailed semantic categories (before and after the observation intervals). This fine-grained change information is more useful in land-cover/land-use (LC/LU) applications. Recent studies indicate that the SCD can be modelled through a triple-branch Convolutional Neural Network (CNN), which contains two temporal branches and a change branch. However, in this architecture, the connections between the temporal branches and the change branch are weak. To overcome these limitations, we propose a novel CNN architecture for the SCD, where the temporal features are re-used and are deeply merged in the temporal branch. Furthermore, we elaborate this architecture to model the bi-temporal semantic correlations. The resulting Bi-temporal Semantic Reasoning Network (Bi-SRNet) contains two types of semantic reasoning blocks to reason both single-temporal and cross-temporal semantic correlations, as well as a novel loss function to improve the semantic consistency of change detection results. Experimental results on a benchmark dataset show that the proposed architecture obtains significant accuracy improvements over the existing approaches, while the added designs in the Bi-SRNet further improves the segmentation of both semantic categories and the changed areas. The codes in this paper are accessible at: <https://github.com/ggsDing/Bi-SRNet>.

1. Introduction

Change detection (CD) refers to the task of identifying the areas in remote sensing images (RSIs) where changes have occurred during the observation intervals [4]. CD is useful for various kinds of real-world applications, such as urban management, environment monitoring, crop monitoring and damage assessment. Although standard CD algorithms allow us to automatically monitor and analyze the region of interests in RSIs, the information provided is coarse-grained and does not describe the detailed change types. In many applications we are interested in not only 'where' the changes occurred, but also 'what' are the changes. To overcome this limitation, semantic change detection (SCD) aims to segmenting the changed areas, as well as providing the semantic categories before and after the change [7].

Recently with the development of Convolutional Neural Networks (CNNs) [21], great improvements have been achieved in terms of CD. Instead of extracting difference information (which is the common practice in expert knowledge-based methods), CNNs learn to directly segment multi-temporal images [30]. CNNs typically have a hierarchy bottom-up design, where the bi-temporal features are embedded and

down-scaled through stacked convolutional layers. The change information is modelled through weighted combination and transformation of the features. Compared with expert knowledge-based methods, CNN-based methods have the advantages of: i) Improved robustness. The CNN-based CD methods are free of hyper-parameters (e.g., weights and thresholds) and can stably process large volumes of data; ii) Modelling more complex changes. CNNs can learn to model some complex change types which can not be well described by hand-crafted features.

However, the SCD of RSIs has been rarely studied in existing works due to its complexity. In the perspective of image processing, CD is essentially a binary segmentation task where a binary map is produced to represent the changed/unchanged regions. However, the SCD is a complex task containing two underlying sub-tasks: i) Semantic segmentation (SS) of the land-cover (LC)/land-use (LU) classes. It is required to segment the bi-temporal semantic labels of either all the RSI or the changed areas; ii) binary CD of the changed areas. Therefore, the results of SCD should be either two temporal LC/LU maps and a change map [7] or two semantic change maps [41]. Previous CNN-based CD methods may not be suitable for the SCD, since they typically contain only a single branch to embed the difference features [6]. Although several recent works have proposed task-specific methods for the SCD [7, 41], they are based on a triple-branch architecture where the sub-tasks are separately modelled. Moreover, the intrinsic correlations between the two sub-tasks have not been considered.

To fill the research gap in SCD, in this paper, we investigate to reason the spatial and temporal semantic correlations

[★]This document is funded by the National Natural Science Foundation of China (No. 41876105, 41671410). It is also funded by the scholarship from China Scholarship Council (grant NO.201703170123).

*Corresponding author

**Principal Corresponding author

✉ lei.ding@unitn.it (D. Lei); ghtgjp2002@163.com (G. Haitao);
sicongliu.rs@gmail.com (L. Sicong); lichao.mou@dlr.de (M. Lichao);
jing.zhang-1@studenti.unitn.it (Z. Jing); lorenzo.bruzzone@unitn.it (L. Bruzzone)

ORCID(s):

in SCD to improve the accuracy. The major contributions in this paper are as follows:

1. Proposing a novel CNN-based architecture for the SCD. The sub-tasks in SCD (SS and CD) are disentangled, whereas their features are shared and are deeply fused. The loss functions are also dis-entangled to supervise respectively SS and CD in the SCD. The resulting architecture shows significant accuracy improvements over existing approaches;
2. Proposing a Bi-temporal Semantic Reasoning Network (Bi-SRNet) for the SCD. Building on top of the novel CNN architecture, the Bi-SRNet further integrates i) two Siamese Semantic Reasoning (Siam-SR) blocks to model the semantic information in each temporal branch, ii) a Cross-temporal SR (Cot-SR) block to model the temporal correlations, and iii) a Semantic Consistency Loss (SCLoss) function to align the semantic and change representations. These designs are verified in an ablation study, whereas the resulting Bi-SRNet is evaluated in comparisons with state-of-the-art (SOTA) methods.

The remainder of this paper is organized as follows. Section 2 introduces the literature works on CD of RSIs. Section 3 elaborates on the proposed CNN architecture, as well as the Bi-SRNet. Section 4 describes the experimental settings and the evaluation metrics. Section 5 reports the results of ablation study and comparative experiments. Section 6 summarizes this work and draws the conclusions.

2. Related Work

This section is organized following the development of CD methods. The pre-CNN and CNN-based methods are separately introduced. Recent methods for the SCD are also reviewed.

2.1. Expert knowledge-based Change Detection

In the past decades, CD techniques have experienced a rapid development owing to the increasing availability of remote sensing images, the successful CD applications, and to the evolution of machine learning. There are many excellent review works in literature (e.g., [34, 22, 1, 19]), focusing on the analyzing of typical CD problems and corresponding methods. Among the traditional expert knowledge-based CD techniques, for the unsupervised CD, in [5], the univariate image differencing and thresholding segmentation was used for solving a binary CD problem from a statistical modeling of the change intensity point of view. Change Vector Analysis (CVA) [23, 2] and its different variation versions (e.g., [3, 16, 18]) promoted the theoretical definition for a CD problem and provide successful solutions for CD in multispectral and hyperspectral images. Another popular transformation-based unsupervised CD approach is the Multivariate Alteration Detection (MAD) [29] and its Iterative reweighted version (IR-MAD) [28], which exploits the nature of changes that exhibited in multiple spectral bands. For the supervised CD, CD approaches are usually designed

by taking advantages of the advanced and robust supervised classifiers such as the Support Vector Machine (SVM), the Random Forest (RF) and the Extreme Learning Machine (ELM) in order to achieve better CD performance with a high accuracy [27, 40, 38]. Other attempts developed from the semi-supervised perspective also greatly joint the merits from both unsupervised and supervised methods in order to improve the automation and robustness of the CD process [49, 20]. On the other hand, CD performance can be also enhanced by considering different features, for example the spectral-spatial features [17], the kernel-based features [36], and the target-driven features [10]. However, the conventional hand-designed features usually represent the low-level descriptions of the change objects, the use of deep learning based approaches provides the capability to learn more complex and effective high-level change features from the data.

2.2. CNN-based Change Detection

The development of convolutional neural networks (CNNs) in the field of computer vision provides insights into change detection. By taking change detection in hyper/multi-spectral imagery as a classification task, [48] presents a 2D CNN to learn spectral-spatial feature representation for this task, and [24] proposes a recurrent CNN that is able to learn spectral-spatial-temporal features and produce good results. Further, in [35], the authors introduce 3D CNN. For high spatial resolution remote sensing images, change detection is usually deemed as a dense prediction problem and solved by semantic segmentation CNNs. For instance, in [7], several Siamese U-Nets are designed for semantic change detection with very high resolution images. The authors of [30] employ an improved UNet++ for this task. [45] presents a network with a hierarchical supervision. In [44], the authors introduce a Siamese CNN to extract features of bi-temporal images and utilize a weighted contrastive loss to alleviate the influence of imbalanced data. To tackle pseudo changes caused by seasonal transitions in change detection tasks, [50] proposes a metric learning-based generative adversarial network (GAN), termed MeGAN, to learn seasonal invariant feature representations. In addition, some works recently focus on devising novel CNN architectures for unsupervised change detection [32, 15, 14, 42, 37, 43, 12].

2.3. Semantic Change Detection

Standard CD outputs binary maps to present the change information, which is often not informative enough in practical applications. There can be multiple change types, such as seasonal changes, urbanization, damages, deforestation and pollution. To elaborate the change information, Multi-class Change Detection [27, 16] (MCD) not only detects the changes, but also classifies the change types. One of the representative CNN-based methods for MCD is the work in [24] which integrates RNN units into CNN: the CNNs are employed to extract spatial information, whereas the RNN units detect multi-class changes from temporal features.

The concept of semantic change detection is first introduced in [13] to describe street-view changes. It extends the

concept of the MCD to consider more change types. Differently from the MCD, the SCD can present both the pre-event and after-event LC/LU information. The complexity in SCD greatly increases, which raises challenges to the algorithms. Common CD methods may fail to process SCD task, since they are commonly designed to capture the difference information. In [6] two SCD methods with triple embedding branches are introduced. Two of the branches segment temporal images into LC/LU maps, while a CD branch detects the difference information. In [41], the triple-branch CNN is further extended by introducing gating and weighting designs in the decoders to improve the feature representations. In this work, a benchmark dataset for the SCD is also released together with task-specific evaluation metrics. However, to the best of our knowledge, limited researches have been conducted for the SCD.

3. Proposed Bi-temporal Semantic Reasoning Network (Bi-SRNet) for SCD

In this section we introduce the Bi-SRNet for SCD. First, we summarize the existing CNN approaches for the SCD and introduce a novel task-specific architecture. Then, we introduce the Bi-SRNet built on top of this proposed SCD architecture. Finally, we introduce the semantic reasoning designs and the loss functions in the Bi-SRNet.

3.1. Task Formulation and Possible Approaches

Before introducing the proposed approach, let us first analysis the task of semantic change detection (SCD) and its connections with the semantic segmentation (SS) and the standard change detection (CD). Given an input image I , the task of SS is to find a mapping function f_s that projects I into a semantic map P :

$$f_s(p_{i,j}) = c_{i,j} \quad (1)$$

where $p_{i,j}$ is a pixel on I , $c_{i,j}$ is the projected LC/LU class. Meanwhile, a standard CD function f_{cd} projects two temporal images I_1, I_2 into a binary change map C :

$$f_{cd}(p_{1,i,j}, p_{2,i,j}) = \begin{cases} 0, & c_{1,i,j} = c_{2,i,j} \\ 1, & c_{1,i,j} \neq c_{2,i,j} \end{cases} \quad (2)$$

where the projected signal (0 or 1) reports if there is change in terms of LU/LC classes or other change types (e.g., damage and status change). The SCD function f_{scd} is a combination of f_s and f_{cd} :

$$f_{scd}(p_{1,i,j}, p_{2,i,j}) = \begin{cases} (0, 0), & c_{1,i,j} = c_{2,i,j} \\ (c_{1,i,j}, c_{2,i,j}), & c_{1,i,j} \neq c_{2,i,j} \end{cases} \quad (3)$$

that produces two semantic change maps S_1 and S_2 .

An intuitive approach to the SCD is to first perform SS and then assign the *non-change* category by logical comparisons between the semantic maps P_1 and P_2 . However, this approach has been proved inferior since the change information is not directly modeled [7]. Alternatively, we employ

CNNs to learn the semantic changes. The possible CNN-based approaches can be summarized as follows:

1) *Direct SCD, early fusion* (DSCD-e, Fig.1(a)). The temporal images I_1 and I_2 are concatenated as input data. A single CNN encoder E is employed to directly learn the f_{scd} :

$$S_1, S_2 = E(I_1, I_2). \quad (4)$$

Many literature works that treat CD as a semantic segmentation task can be divided into this category, including the FC-EF in [6] and the UNet++ in [30]. A major limitation of this architecture is that bi-temporal semantic information is not fully exploited. Since the changed areas are minority, E is driven to pay more attention to the unchanged areas.

2) *Direct SCD, late fusion* (DSCD-l, Fig.1(b)). I_1 and I_2 are separately fed as inputs into two CNN encoders E_1 and E_2 (which can be weight-sharing, i.e., siamese [6], if I_1 and I_2 belong to the same domain). The encoded features are then fused and modelled through a convolutional CD unit D . E_1 and E_2 serve as feature extractors, whereas the f_{scd} is learned by D with the embedded semantic features:

$$S_1, S_2 = D[E(I_1), E(I_2)]. \quad (5)$$

This architecture may also include decoder networks and skip connections. In the FC-Siam-conc. and the FC-Siam-diff. [6] the CD units are multi-scale concatenation blocks, whereas in the ReCNN[24] they are Recurrent Neural Networks (RNNs). However, the extraction of semantic information is still insufficient in this architecture. The *non-change* class is still competing with other classes during the network inference, which does not correctly reflect their intrinsic correlations.

3) *Disentangled SS and CD, early fusion* (SSCD-e, Fig.1(c)). Three CNN encoders E_1 , E_2 and E_c are separately trained with I_1 , I_2 and (I_1, I_2) as the inputs. E_1 and E_2 can be siamese if I_1 and I_2 belong to the same domain. The semantic and change information are separately modelled. E_1 and E_2 produce the semantic maps P_1 and P_2 , while E_c produces a binary change map C . S_1, S_2 are then generated by masking P_1, P_2 with C . The calculations are as follows:

$$P_1, P_2, C = E_1(I_1), E_2(I_2), E_c(I_1, I_2) \quad (6)$$

$$S_1, S_2 = C \cdot (P_1, P_2). \quad (7)$$

A representative of this architecture is the HRSCD-str.3 in [7]. However, a disadvantage of this architecture is insufficient communications between the temporal branches and the change branch. Although there can be connections between E_1 , E_2 and E_c (e.g., the skip-connections in the HRSCD-str.4 [7] and the gating operations in the ASN [41]), the semantic features are still not fully re-used and are not deeply merged. Additionally, training the f_{cd} from scratch with input images is not computation-efficient.

4) *Disentangled SS and CD, late fusion* (SSCD-l, Fig.1(c)). This is a novel architecture proposed to address the limitations of above-mentioned approaches. In the SSCD-l, two

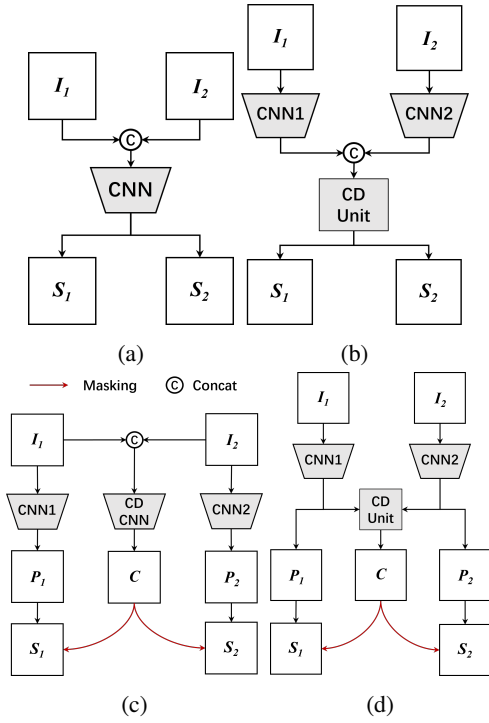


Figure 1: 4 possible CNN architectures for the SCD: (a) Direct SCD, early fusion (DSCD-e); (b) Direct SCD, late fusion (DSCD-l); (c) Disentangled SS and CD, early fusion (SSCD-e); and (d) Disentangled SS and CD, late fusion (SSCD-l).

CNN encoders E_1 and E_2 are employed to extract semantic information from I_1 and I_2 . The extracted semantic features are further merged to train a CD unit D , which exploits the difference information. The calculations can be represented as follows:

$$P_1, P_2 = E_1(I_1), E_2(I_2) \quad (8)$$

$$C = D[E(I_1), E(I_2)] \quad (9)$$

$$S_1, S_2 = C \cdot (P_1, P_2). \quad (10)$$

The advantages of the SSCD-l architecture are two-fold: i) Both the semantic information and the change information are explicitly modelled. This enables the SSCD-l to embed more oriented features for the underlying sub-tasks (SS and CD); ii) The change information is learned uniformly in the CD branch instead of being modelled separately in each temporal branch (such as in the DSCD-e and the DSCD-l). This results in consistent change information across the two temporal predictions S_1 and S_2 ; iii) Semantic features from the two temporal branches are re-used and are deeply merged through D . In this way D is aware of the semantic information.

To find out the optimal CNN architecture for the SCD, experimental comparisons have been conducted in Section 5.1 and Section 5.3.

3.2. Bi-temporal Semantic Reasoning Network

In the proposed SSCD-l architecture, the semantic features are separately extracted through two temporal branches

and are deeply merged through the CD unit. However, one of the remaining problems is to model the temporal coherence between the two feature extraction branches. The majority of image regions remain unchanged through the observation intervals, thus they exhibit similar visual patterns. To better exploit this information, we propose the Bi-temporal Semantic Reasoning Network (Bi-SRNet) as illustrated in Fig.2.

The Bi-SRNet is built on top of the SSCD-l architecture by introducing two extra Semantic Reasoning (SR) blocks [25, 47] and a semantic consistency loss. Given 2 input temporal images I_1 and I_2 , the Bi-SRNet first employs 2 CNN encoders E_1 and E_2 to extract the semantic features X_1 and X_2 . Differently from the SSCD-l, X_1 and X_2 are then processed by two Siamese SR (Siam-SR) blocks to improve their semantic representations. Under the circumstance that there is no significant domain difference, the weights of both E_1, E_2 and the Siam-SRs are shared to reduce over-fitting risks. The enhanced features X'_1 and X'_2 are further sent to a Cross-temporal SR (Cot-SR) block to model their semantic correlations. These correlations between the two temporal branches are also supervised by the semantic consistency loss (introduced in Section 3.4). The temporally aligned features X''_1 and X''_2 are then projected into two semantic maps P_1 and P_2 . Meanwhile, the CD block models change information through the unaligned features X'_1 and X'_2 , before them being projected into a binary change map C . All the projections are made through 1×1 convolutional layers whose weights are not shared. Same as the SSCD-l, the Bi-SRNet outputs 3 direct results: the semantic maps P_1, P_2 and a binary CD map C . Finally, the semantic change maps S_1 and S_2 are generated by masking P_1 and P_2 with C . E_1, E_2 and D in the Bi-SRNet are identical to those in the SSCD-l. The simplified calculations (omitting the convolutional classifiers) are:

$$\hat{X}_1 = \text{SiamSR}[E_1(I_1)], \hat{X}_2 = \text{SiamSR}[E_2(I_2)] \quad (11)$$

$$P_1, P_2 = \text{CotSR}(\hat{X}_1, \hat{X}_2) \quad (12)$$

$$C = D(\hat{X}_1, \hat{X}_2) \quad (13)$$

$$S_1, S_2 = C \cdot (P_1, P_2). \quad (14)$$

Since the focus of this work is to investigate architecture designs and to model the semantic correlations for SCD, no decoder structures are adopted. The SR blocks operate on a spatial scale of $1/8$ of the input resolution. The network outputs are directly enlarged as the results.

3.3. Semantic Reasoning Blocks

Non-local units [39] have been proved effective to model long-range dependencies in images and have been widely used in semantic segmentation tasks [26, 25, 47]. In the SCD task it is beneficial to take into account both i) the spatial correlations within each temporal image and ii) the semantic consistency between the bi-temporal images. In the Bi-SRNet these information are learned through the Siam-SR blocks and the Cot-SR block, respectively.

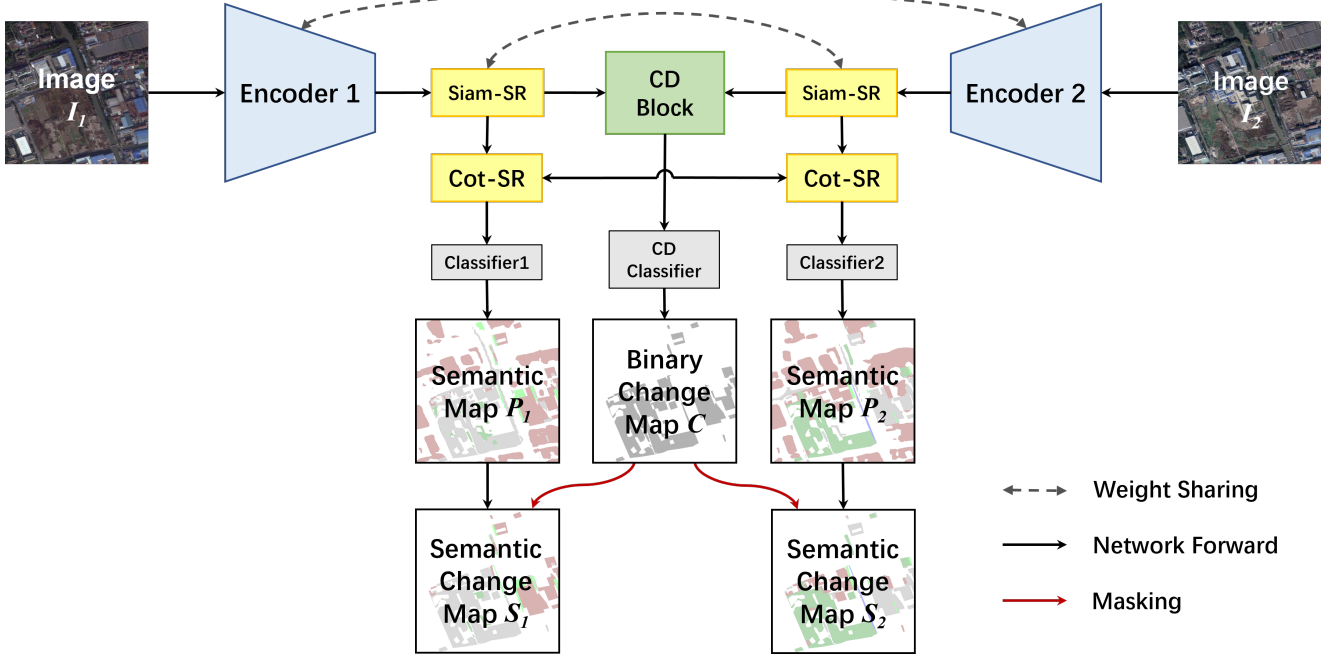


Figure 2: Architecture of the proposed Bi-temporal Semantic Reasoning Network (Bi-SRNet) for SCD. The modelling of semantic and changed information is disentangled to enhance the feature exploitation, whereas the semantic representations in the two temporal branches are aligned through the SR blocks.

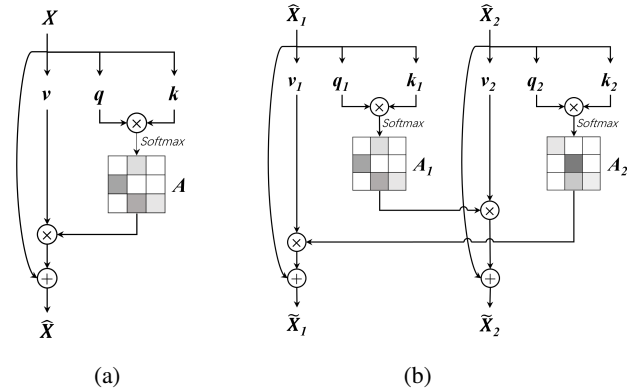


Figure 3: Structures of the (a) Siamese Semantic Reasoning (Siam-SR) and (b) Cross-temporal Semantic Reasoning (Cot-SR) blocks.

The Siam-SR blocks are two standard non-local units that share the same weights. Fig.3(a) illustrates the operations inside a Siam-SR block. Given an input feature $\mathbf{X} \in \mathbb{R}^{c \times h \times w}$, a Siam-SR block first projects it into three vectors $\mathbf{q} \in \mathbb{R}^{N \times c'}$, $\mathbf{k} \in \mathbb{R}^{c' \times N}$ and $\mathbf{v} \in \mathbb{R}^{c \times N}$, where $N = hw$ and $c' = c/r$, r is a channel reduction factor (normally set to 2). An attention matrix $\mathbf{A} \in \mathbb{R}^{N \times N}$ is then calculated as:

$$\mathbf{A} = \phi(\mathbf{q} \times \mathbf{k}) \quad (15)$$

where ϕ is a *softmax* normalization function along the row dimension. \mathbf{A} records the correlations between each pair of spatial positions. An enhanced feature $\hat{\mathbf{X}}$ is then obtained

with:

$$\hat{\mathbf{X}} = \mathbf{X} + \mathbf{v} \times \mathbf{A} \quad (16)$$

Intuitively, the bi-temporal information provides more clues of the image context. Therefore, we propose the Cot-SR block, which is an extension of the non-local unit to model cross-temporal information. As illustrated in Fig.3(b), the Cot-SR block simultaneously enhances two temporal features $\hat{\mathbf{X}}_1, \hat{\mathbf{X}}_2 \in \mathbb{R}^{c \times h \times w}$. First, 6 vectors $\mathbf{q}_1, \mathbf{q}_2 \in \mathbb{R}^{N \times c'}$, $\mathbf{k}_1, \mathbf{k}_2 \in \mathbb{R}^{c' \times N}$ and $\mathbf{v}_1, \mathbf{v}_2 \in \mathbb{R}^{c \times N}$ are projected from $\hat{\mathbf{X}}_1$ and $\hat{\mathbf{X}}_2$. Second, two attention matrices $\mathbf{A}_1, \mathbf{A}_2 \in \mathbb{R}^{N \times N}$ are generated to record the semantic focuses in each temporal branch:

$$\mathbf{A}_1 = \phi(\mathbf{q}_1 \times \mathbf{k}_1) \quad (17)$$

$$\mathbf{A}_2 = \phi(\mathbf{q}_2 \times \mathbf{k}_2) \quad (18)$$

Finally, each attention map operates on its opposite temporal branch to project cross-temporal correlations:

$$\tilde{\mathbf{X}}_1 = \hat{\mathbf{X}}_1 + \mathbf{v}_1 \times \mathbf{A}_2 \quad (19)$$

$$\tilde{\mathbf{X}}_2 = \hat{\mathbf{X}}_2 + \mathbf{v}_2 \times \mathbf{A}_1 \quad (20)$$

where $\tilde{\mathbf{X}}_1, \tilde{\mathbf{X}}_2$ are the enhanced features.

The Siam-SR blocks aggregate spatial information to embed semantic focuses into each temporal branch, whereas the Cot-SR learns cross-temporal semantic consistency to enhance the features in unchanged areas.

3.4. Loss Functions

We use three loss functions to train the Bi-SRNet: the semantic loss \mathcal{L}_{sem} , the change loss \mathcal{L}_{change} , and a proposed semantic consistency loss \mathcal{L}_{sc} .

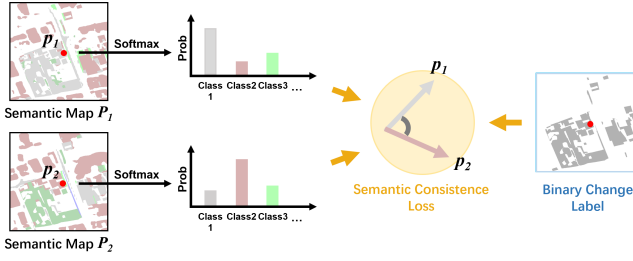


Figure 4: Illustration of the calculation of the Semantic consistency Loss (SCLoss).

The semantic loss \mathcal{L}_{sem} is the multi-class cross entropy loss between the semantic segmentation results P_1, P_2 and the GT semantic maps L_{S1}, L_{S2} . The calculation of \mathcal{L}_{sem} on each pixel is:

$$\mathcal{L}_{sem} = -\frac{1}{N} \sum_{i=1}^N y_i \log(p_i) \quad (21)$$

where N is the number of semantic classes, y_i and p_i denote the GT label and the predicted probability of the i -th class, respectively. Under the circumstance that there are only semantic change labels L_1 and L_2 available, they can be alternatives to L_{S1} and L_{S2} by restricting the semantic supervisions on changed areas only. In that case, the *non-change* class (at index '0') on L_1 and L_2 are excluded from calculation, thus formula (21) stays the same.

The change loss \mathcal{L}_{change} is the binary cross entropy loss between the predicted binary change map C and the reference change map L_c . If L_c is not given, it can be easily obtained from L_1 or L_2 by replacing all the semantic labels with a *changed* label. The \mathcal{L}_{change} for each pixel is calculated as:

$$\mathcal{L}_{change} = -y_c \log(p_c) - (1 - y_c) \log(1 - p_c) \quad (22)$$

where y_c and p_c denote the GT label and the predicted probability of change, respectively.

\mathcal{L}_{sem} and \mathcal{L}_{change} are designed to improve the semantic embedding and the CD, respectively. We further propose a task-specific semantic consistency loss (SCLoss) to link SS with CD. It aligns the semantic representations between the two temporal branches, as well as guides training of the Cot-SR block. As illustrated in Fig.4, the SCLoss awards predictions with similar probability distributions in the *non-change* areas, whereas punishing those in the changed areas. This fits the intrinsic temporal correlations in the SCD task. The SCLoss \mathcal{L}_{sc} is calculated between the predicted semantic maps P_1, P_2 and the change label L_c using the Cosine loss function:

$$\mathcal{L}_{sc} = \begin{cases} 1 - \cos(x_1, x_2), & y_c = 1 \\ \cos(x_1, x_2), & y_c = 0 \end{cases} \quad (23)$$

where x_1, x_2 are feature vectors of a pixel on P_1 and P_2 , respectively. y_c is the value at the same position on L_c .

Training of the two feature embedding branches is directly supervised by L_1 and L_2 and is assisted by L_c (through

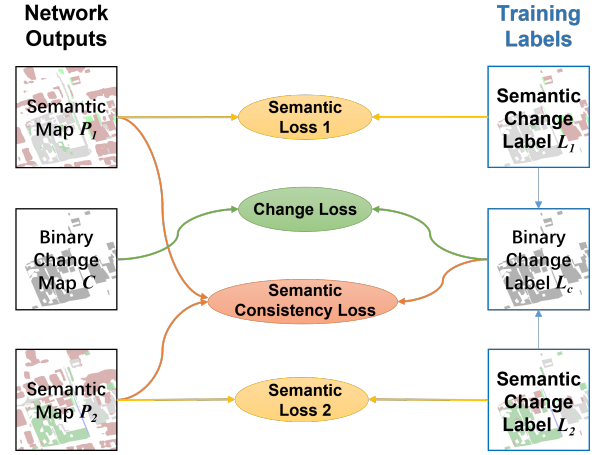


Figure 5: The calculation of supervision losses in the Bi-SRNet.

the \mathcal{L}_{sc}), while training of the CD block is directly supervised by L_c . The relationships between the 3 outputs P_1, P_2, C and the GT maps L_1, L_2 and L_c are illustrated in Fig.5. The total loss \mathcal{L}_{scd} is calculated as:

$$\mathcal{L}_{scd} = \alpha \mathcal{L}_{sem} + \mathcal{L}_{change} + \mathcal{L}_{sc} \quad (24)$$

where α is a weighting parameter normally set to 0.5.

4. Dataset Description and Experimental Settings

In this section we describe the experimental settings, dataset and the evaluation metrics.

4.1. Dataset

The experiments in this study are conducted on the Semantic Change detection Dataset (SECOND)[41], a benchmark dataset for the SCD. The SECOND are constructed with bi-temporal HR optical images (containing RGB channels) collected by aerial platforms. The observed regions include several cities in China, including Hangzhou, Chengdu and Shanghai. Each image has the same spatial size of 512×512 pixels.

The LC categories before and after the change events are provided. In each GT semantic change map, 1 change class and 6 LC classes are annotated, including: *non-change, non-vegetated ground surface, tree, low vegetation, water, buildings* and *playgrounds*. The Bi-temporal semantic change maps are related to around 30 types of LC changes. Among the 4662 pairs of temporal images, 2968 ones are openly available. We further split them into a training set and as testing set with the numeric ratio of 9 : 1 (i.e., 2672 image pairs for training, 296 ones for testing).

4.2. Evaluation Metrics

In this study, 3 evaluation metrics are adopted to evaluate the SCD accuracy, including: overall accuracy (OA), mean Intersection over Union (mIoU) and Separated Kappa

(SeK) coefficient. OA has been commonly adopted in both semantic segmentation [9, 8] and CD [7] tasks. Let us denote $Q = \{q_{i,j}\}$ as the confusion matrix where $q_{i,j}$ represents the number of pixels that are classified into i while their GT index is j ($i, j \in \{0, 1, \dots, N\}$, 0 represents class *non-change*). OA is calculated as:

$$OA = \sum_{i=0}^N q_{ii} / \sum_{i=0}^N \sum_{j=0}^N q_{ij}. \quad (25)$$

Since OA is mostly determined by the identification of *non-change* pixels, it cannot well evaluate the segmentation of LC/LU classes. Additionally, it does not count the pixels that are identified as *changed* but are predicted into wrong LC/LU classes. Alternatively, mIoU and SeK are suggested in the SECOND [41] to evaluate the discrimination of *changed/non-change* regions and the segmentation of LC classes, respectively.

mIoU is the mean value of the IoU of *non-change* regions (IoU_{nc}) and that of the *changed* regions (IoU_c):

$$mIoU = (IoU_{nc} + IoU_c) / 2, \quad (26)$$

$$IoU_{nc} = q_{00} / (\sum_{i=0}^N q_{i0} + \sum_{j=0}^N q_{0j} - q_{00}), \quad (27)$$

$$IoU_c = \sum_{i=1}^N \sum_{j=1}^N q_{ij} / (\sum_{i=0}^N \sum_{j=0}^N q_{ij} - q_{00}), \quad (28)$$

The SeK coefficient is calculated based on the confusion matrix $\hat{Q} = \{\hat{q}_{ij}\}$ where $\hat{q}_{ij} = q_{ij}$ except that $\hat{q}_{00} = 0$. This is to exclude the true positive *non-change* pixels, whose number is dominant. The calculations are as follows:

$$\rho = \sum_{i=0}^N \hat{q}_{ii} / \sum_{i=0}^N \sum_{j=0}^N \hat{q}_{ij}, \quad (29)$$

$$\eta = \sum_{i=0}^N (\sum_{j=0}^N \hat{q}_{ij} * \sum_{j=0}^N \hat{q}_{ji}) / (\sum_{i=0}^N \sum_{j=0}^N \hat{q}_{ij})^2, \quad (30)$$

$$SeK = e^{IoU_c - 1} \cdot (\rho - \eta) / (1 - \eta). \quad (31)$$

The mIoU and SeK directly evaluate the sub-tasks in SCD, i.e., the CD and the SS of LC/LU classes, respectively.

Additionally, three metrics are provided to measure the computational costs, including the size of parameters (Params.), the floating point operations (FLOPs) and the inference (Infer.) time for 100 epochs. The FLOPs and Infer. time are measured considering the calculations for a pair of input images each with 512×512 pixels.

4.3. Experimental settings

The experiments in this study are conducted on a workstation with a NVIDIA Quadro P6000 GPU. All the CNN models are implemented with the PyTorch library. The same experimental parameters are used in all the experiments, including batch size (8), running epochs (50) and initial learning (0.1). The gradient descent optimization method is Stochastic Gradient Descent (SGD) with Nesterov momentum. The

augmentation strategy include random flipping and rotating while loading the image pairs. For simplicity, no test-time augmentation operation is applied.

5. Experimental Results

In this section, a series of experiments are conducted to verify the effectiveness of the proposed architecture for SCD (the SSCD-l) and the components in the Bi-SRNet. Finally the proposed methods are compared with several recent methods in both SCD and binary CD.

5.1. Comparison of SCD Architectures

To find the optimal CNN architecture for the SCD, we compare the 4 approaches discussed in Section 3.1: the DSCD-e, DSCD-l, SSCD-e and SSCD-l. For simplicity and fairness, all the tested architectures are implemented with only the basic convolutional designs (i.e., sophisticated designs such as encoder-decoder structures, dilated convolutions and attention units are not adopted). They employ the same CNN encoder (the ResNet34 [11]), adopt the same down-sampling stride ($\times 1/8$) and have same number of inner channels at each convolutional stage. The late-fusion approaches (DSCD-e and SSCD-l) employ an identical CD block, i.e., a CNN block with 6 stacked residual units.

The quantitative results are reported in Table.5.1. The DSCD-e architecture obtains the lowest accuracy, although it requires the lowest computations. Meanwhile, DSCD-l obtains much higher metrics, showing that the separate embedding of temporal features and CD features is essential in SCD. Compared to the DSCD-l, the SSCD-e increases slightly the mIoU values at the cost of taking much heavier computations. This shows that the embedding of CD features from scratch is in-efficient. On the contrast, the proposed SSCD-l re-uses and merges the temporal features for CD, which leads to significant performance improvements. It surpasses the SSCD-e by over 3% in mIoU and 5% in SeK, whereas its computational costs are only slightly higher than those of the DSCD-l.

These experimental comparisons indicate that the proposed SSCD-l is optimal for SCD among the compared standard forms of architectures. Its advantages in embedding the semantic information (indicated by the SeK) is particularly dominant. However, there are also many variants of these architectures in previous studies. In Section 5.3 these methods are further compared to summarize common features of the different SCD architectures.

5.2. Ablation Study

After verifying the effectiveness of the SSCD-l, we further perform an ablation study to evaluate the auxiliary components in the proposed Bi-SRNet. The quantitative results are presented in Table.5.2. First we test the effectiveness of the SCLoss by adding it as an auxiliary loss to train the SSCD-l. This boosts the accuracy by around 0.2% in SeK and 0.14% in OA, indicating that the semantic embedding of features are improved. Taking this method (SSCD-l with SCLoss) as the baseline, we further assess the performance

Table 1

Comparison of different CNN architectures for SCD.

Method	Computational Costs			Accuracy		
	Params (Mb)	FLOPS (Gbps)	Infer. Time (s/100e)	mIoU(%)	Sek(%)	OA(%)
DSCD-e	21.36	91.39	1.32	49.83	-1.83	81.73
DSCD-l	23.31	189.54	2.74	68.91	16.48	87.87
SSCD-e	42.72	272.95	3.89	69.54	16.67	86.72
proposed SSCD-l	23.31	189.57	2.75	72.60	21.86	88.24

Table 2

Quantitative results of the ablation study.

Proposed Method	Components				mIoU(%)	Sek(%)	OA(%)
	CD block	siam-SR block	Cot-SR block	SCLoss			
SSCD-l	✓				72.60	21.86	88.24
SCLoss-SSCDl	✓			✓	72.69	22.03	88.38
SiamSR-SSCDl	✓	✓		✓	72.84	22.37	88.48
CotSR-SSCDl	✓		✓	✓	72.73	22.35	88.49
Bi-SRNet	✓	✓	✓	✓	72.93	22.70	88.72

of each SR block. The Siam-SR blocks, which are placed on each temporal branch, lead to significant accuracy improvements (0.15% in mIoU and over 0.3% in SeK). Meanwhile, the Cot-SR block that models the temporal coherence improves greatly the SeK (by over 0.3%) and the OA (by over 0.1%). This indicates that both the Siam-SR and the Cot-SR improve the semantic embedding of temporal features, while the former also benefits the detection of change information. Finally, we evaluate the Bi-SRNet which contains all these auxiliary designs. Compared to the standard SSCD-l, its improvements are around 0.3% in mIoU, 1% in SeK and 0.5 % in OA. These results indicate that the Bi-SRNet integrating all the designs brings a leap in accuracy.

The qualitative results in some testing areas are presented in Fig.6. The prediction maps from left to right are provided by the proposed methods in Table 5.2, which are organized in the sequence of number of contained components. Compared to the results of the standard SSCD-l, the predicted LC categories after introducing the SCLoss and SR blocks are gradually improved. The Bi-SRNet exhibits great advantages in discriminating the critical areas.

Through this ablation study we find that: i) as indicated by increases in SeK values, all the tested auxiliary components result in noticeable improvements in semantic embedding; ii) the semantic reasoning designs in the Bi-SRNet benefit not only the discrimination of LC categories, but also the detection of changes.

5.3. Comparative Experiments

To comprehensively evaluate the performance of the SSCD-l architecture and the Bi-SRNet, we further compare them with several SOTA methods in both CD and SCD tasks. The compared methods include:

1) *The FC-EF, FC-Siam-conv. and FC-Siam-diff.* [6]. These are three UNet-like[31] CNNs for binary CD. The FC-

EF concatenates temporal images as inputs, whose architecture can be divided into the DSCD-e. The FC-Siam-conv. and FC-Siam-diff. both contain siamese encoders while their decoders also serve as CD blocks, which can be divided into the DSCD-l.

2) *The UNet++* [30]. This model is a variant of the UNet and can be divided into the DSCD-e. Note that the deep supervision function introduced in [30] is not suitable for the SCD task, thus it is removed.

3) *The HRSCD-str.2, HRSCD-str.3 and HRSCD-str.4* [7]. These are three methods introduced for the SCD, both containing residual blocks [11] and encoder-decoder structures. The HRSCD-str.2 directly produce semantic change maps, thus belongs to the type DSCD-e. The HRSCD-str.3 and HRSCD-str.4 both contain triple encoding branches, thus belong to the type SSCD-e.

4) *The ResNet-GRU and ResNet-LSTM* [24]. These methods are derived from the methods in [24] that combines CNN and RNNs for CD. Since the original methods are designed to classify low-resolution RSIs and contain only few convolutional layers, which are not suitable for processing HR RSIs, we further change their encoders into the ResNet34[11]. The RNN units serve as CD blocks, thus these methods belong to the DSCD-l.

5) *The IFN* [46]. This method contains a VGGNet[33] encoder and an attention-based decoder. The features are merged in the decoder, thus it belongs to the DSCD-l.

Among the above-mentioned methods, the ones that in 3) are for the SCD, whereas those in 2), 4) and 5) are originally designed for binary CD. To apply these CD methods for the SCD, we slightly modified their last convolutional layers to meet the required numbers of output maps and channels. The quantitative results are reported in Table 5.3. One can observe the methods using the DSCD-e and the DSCD-l architectures generally produce unsatisfactory results. In

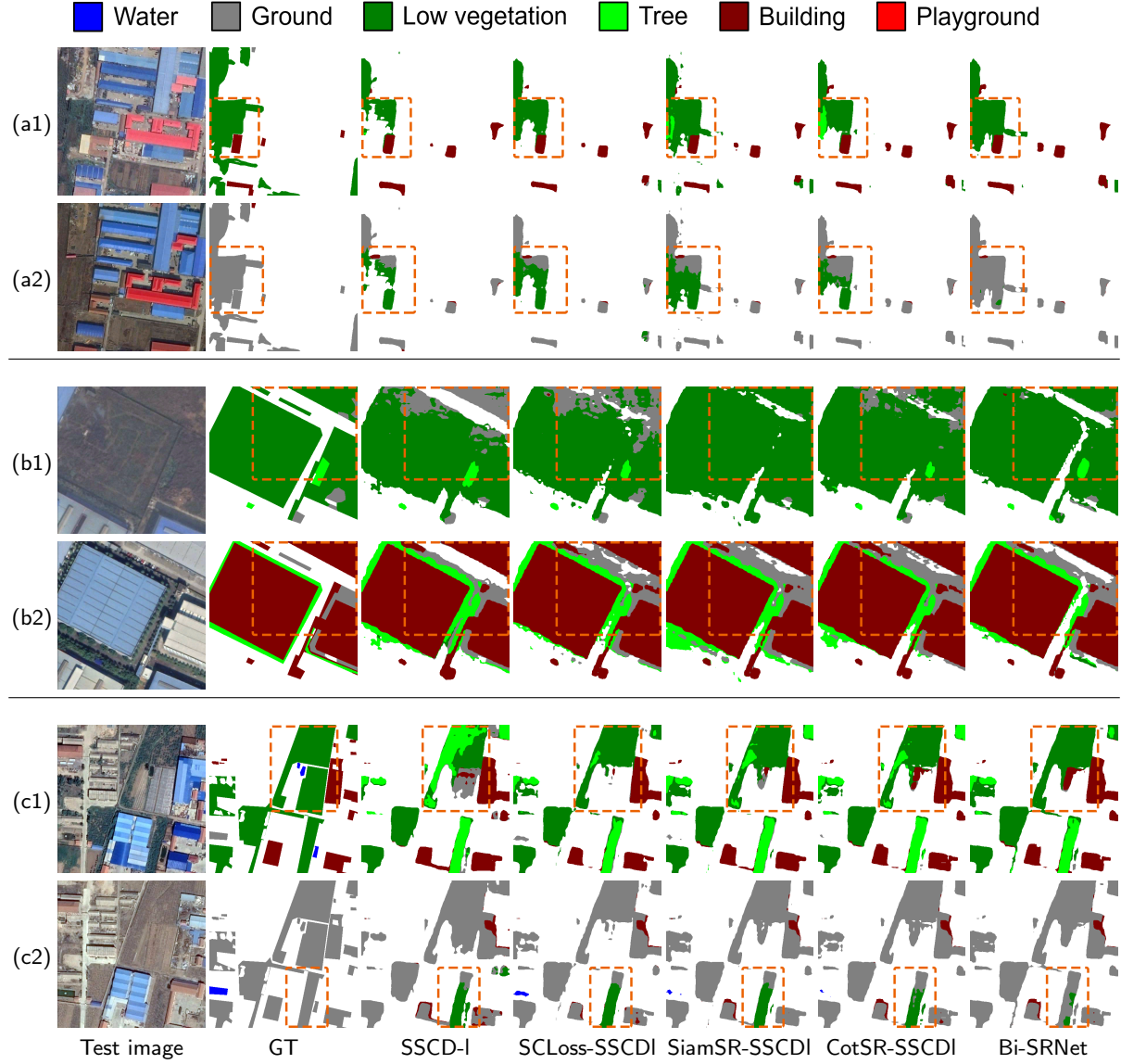


Figure 6: Example results provided by different proposed methods in the ablation study. The major differences are highlighted in orange rectangles.

Table 3

Comparison with literature methods for the SCD.

Method	Arch. Type	Computational Costs			Accuracy		
		Params (Mb)	FLOPs (Gbps)	Infer. Time (s/100e)	mIoU(%)	Sek(%)	OA(%)
FC-EF [6]	DSCD-e	1.66	17.75	0.73	65.38	11.25	86.77
UNet++ [30]	DSCD-e	9.16	139.82	3.46	65.18	10.86	86.46
HRSCD-str.2 [7]	DSCD-e	6.39	14.29	2.33	62.79	1.29	84.03
ResNet-GRU [24]	DSCD-I	21.45	182.36	2.73	66.69	14.94	87.60
ResNet-LSTM [24]	DSCD-I	21.48	182.63	2.73	66.87	14.96	87.56
FC-Siam-conc. [6]	DSCD-I	2.74	35.01	1.21	68.98	16.69	87.98
FC-Siam-diff. [6]	DSCD-I	1.66	21.41	1.02	68.75	16.17	87.93
IFN [46]	DSCD-I	35.73	329.10	9.41	64.59	11.62	87.21
HRSCD-str.3 [7]	SSCD-e	12.77	42.67	6.26	66.86	12.56	85.71
HRSCD-str.4 [7]	SSCD-e	13.71	43.69	6.37	71.53	19.11	87.46
SSCD-I (proposed)	SSCD-I	23.31	189.57	2.75	72.60	21.86	88.24
Bi-SRNet (proposed)	SSCD-I	23.39	189.91	3.42	72.93	22.70	88.72

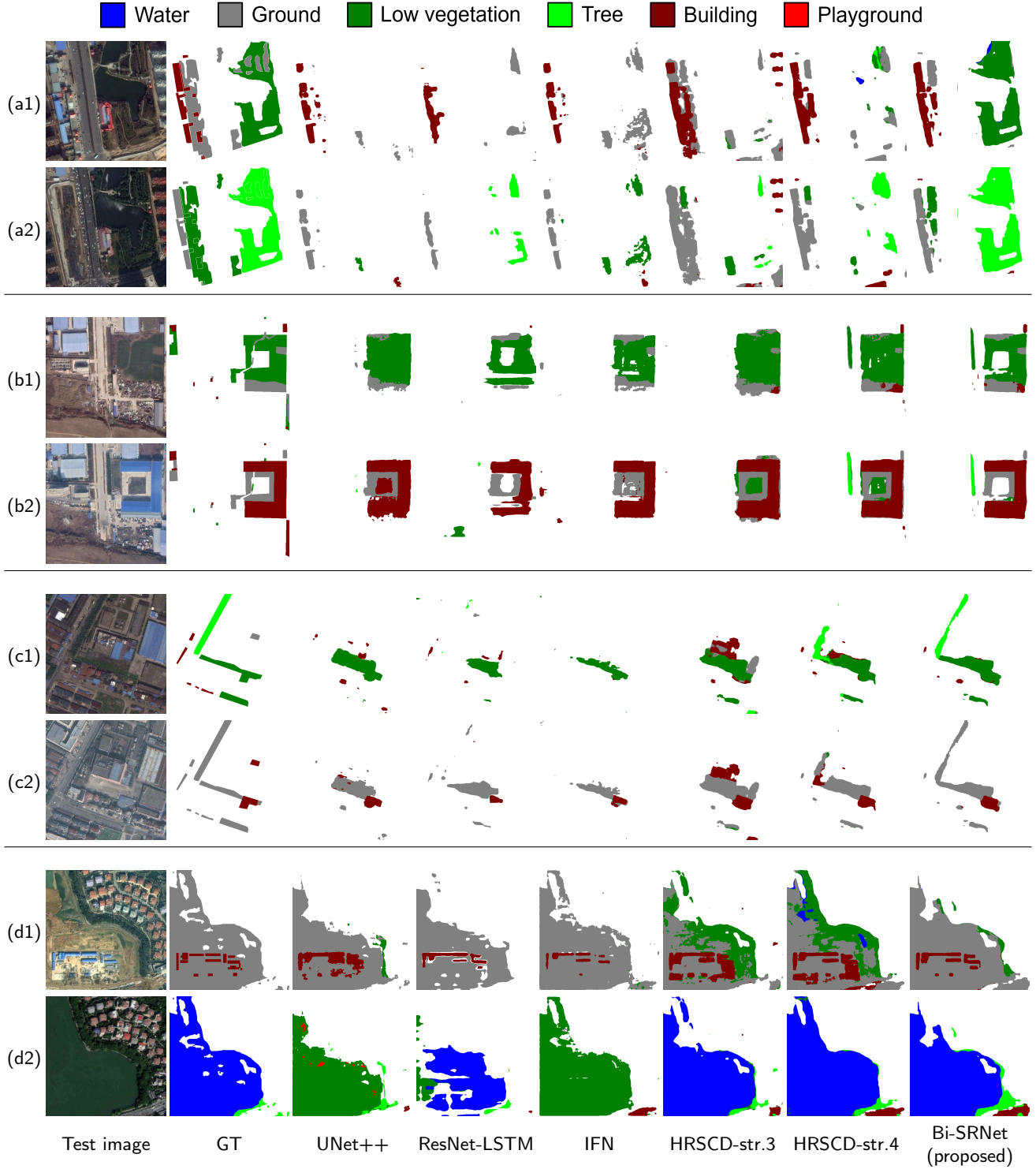


Figure 7: Example results provided by different proposed methods in the comparative experiments.

these methods, the modelling of semantic information and change information is entangled, which leads to low SeK values. Two exceptions are the FC-Siam-conv. and the FC-Siam-diff., which concatenate and merge the semantic features through their decoders. The methods with SSCD-e architectures, particularly the HRSCD-str.4, obtain higher accuracy mIoU and SeK values. The HRSCD-str.4 contains

skip-connections between the temporal branches and the CD branch, which alleviates the drawbacks in the standard SSCD-e and obtains the 3rd-best accuracy. The proposed methods based on the SSCD-l architectures obtain the best accuracy. Without using any CNN decoder or specialized encoder, the proposed Bi-SRNet outperform the SOTA by a large margin on all the metrics (1.4%, 3.6% and 1.3% in mIoU, SeK

and OA, respectively). This confirms that the SSCD-I is the optimal CNN architecture for the SCD.

Additionally, the computational costs of different methods are also reported in Table 5.3. Generally, the models with ResNet34 encoders (ResNet-GRU, ResNet-LSTM, SSCD-I and Bi-SRNet) have more parameter size and require more calculations. However, their inference time is close to some UNet-based methods (e.g., UNet++ and HRSCD-str.2), since most of the calculations are performed on down-scaled feature maps (at Stage 3 and 4 in the ResNet). The HRSCD-str.3 and HRSCD-str.4 that contain intense calculations in the decoder even require more inference time. The IFN that contains also cascaded attention blocks in the decoder requires the most calculations and inference time. Inference time of the proposed methods (SSCD-I and Bi-SRNet) are at the middle level among the compared methods.

To visually assess the results, in Fig.7 we present comparisons of the results provided by different methods in several sample areas. One can observe that most of these methods are sensitive to the semantic changes between *building* and *low vegetation*. However, the DSCD-based methods commonly omit some other LC classes. Specifically, the UNet++, the ResNet-LSTM and the IFN omitted many *tree* and *water* areas. The detection of changes is much improved in SSCD-based results. However, the SSCD-e based approaches (HRSCD-str.3 and HRSCD-str.4) mis-classified the LC classes in some critical areas (e.g., confusion between *ground* and *low vegetation* in Fig.7(d1)) and omitted some minor changes (e.g., the *low vegetation* to *tree* changes in Fig.7(a) and the *tree* to *ground* changes in Fig.7(c)). Meanwhile, these change types are all captured by the proposed Bi-SRNet. This further confirms its advantages in both CD and semantic exploitation.

6. Conclusions

In this study, we investigated to improve the accuracy of SCD task. First, we summarized the existing CNN architectures for SCD and found that there are limitations in semantic embedding and CD. Therefore, we proposed a novel SCD architecture, the SSCD-I, where the semantic features are re-used and deeply merged in a convolutional CD block. Then, we further extend the SSCD-I architecture into the Bi-SRNet by introducing several semantic modelling designs. Three auxiliary designs are introduced, including two Siam-SR blocks to augment temporal information, a Cot-SR block to model temporal correlations, as well as a SCLoss to enhance temporal coherence. Finally, a set of experiments have been conducted to evaluate the effectiveness of the proposed methods.

Through experiments we found that: i) The proposed SSCD-I architecture outperforms other standard SCD architectures by a large margin; ii) The proposed Bi-SRNet containing semantic reasoning designs further improves the SSCD-I in not only the segmentation of LC classes, but also the detection of changes; iii) The SSCD-I based methods (standard SSCD-I and the Bi-SRNet) outperform SOTA methods and obtain the highest accuracy metrics on the SECOND.

The advantages of the Bi-SRNet are two-fold. First, in the SSCD-I architecture, the sub-tasks in SCD (SS and CD) are disentangled (with separate outputs and loss functions) but are deeply integrated (through re-use of the semantic features in the CD block). This leads to more accurate CD results. Second, the spatial and temporal correlations are modelled in the Bi-SRNet with both the SR blocks and the SCLoss. This further bridges the sub-tasks in SCD and enables the Bi-SRNet to discriminate better the LC classes in critical areas.

The focus of this study is to improve the SCD in terms of architecture designs and semantic reasoning. Therefore, more sophisticated designs such as bi-temporal encoder-decoder structures [7], deep supervision [30] and attention-based decoders [46, 41] are not investigated. There is still margin to further improve the classification of LC categories in changed areas, which is left for future studies.

References

- [1] Ban, Y., Yousif, O., 2016. Change Detection Techniques: A Review. Springer International Publishing, Cham. pp. 19–43. doi:10.1007/978-3-319-47037-5_2.
- [2] Bovolo, F., Bruzzone, L., 2007. A theoretical framework for unsupervised change detection based on change vector analysis in the polar domain. IEEE Transactions on Geoscience and Remote Sensing 45, 218–236.
- [3] Bovolo, F., Marchesi, S., Bruzzone, L., 2012. A framework for automatic and unsupervised detection of multiple changes in multitemporal images. IEEE Transactions on Geoscience and Remote Sensing 50, 2196–2212.
- [4] Bruzzone, L., Bovolo, F., 2012. A novel framework for the design of change-detection systems for very-high-resolution remote sensing images. Proceedings of the IEEE 101, 609–630.
- [5] Bruzzone, L., Prieto, D.F., 2000. Automatic analysis of the difference image for unsupervised change detection. IEEE Transactions on Geoscience and Remote Sensing 38, 1171–1182.
- [6] Daudt, R.C., Le Saux, B., Boulch, A., 2018. Fully convolutional siamese networks for change detection, in: 2018 25th IEEE International Conference on Image Processing (ICIP), IEEE. pp. 4063–4067.
- [7] Daudt, R.C., Le Saux, B., Boulch, A., Gousseau, Y., 2019. Multitask learning for large-scale semantic change detection. Computer Vision and Image Understanding 187, 102783.
- [8] Ding, L., Bruzzone, L., 2020. Diresnet: Direction-aware residual network for road extraction in vhr remote sensing images. IEEE Transactions on Geoscience and Remote Sensing .
- [9] Ding, L., Tang, H., Bruzzone, L., 2020. Lanet: Local attention embedding to improve the semantic segmentation of remote sensing images. IEEE Transactions on Geoscience and Remote Sensing 59, 426–435.
- [10] Du, P., Liu, S., Bruzzone, L., Bovolo, F., 2012. Target-driven change detection based on data transformation and similarity measures, in: 2012 IEEE International Geoscience and Remote Sensing Symposium, pp. 2016–2019. doi:10.1109/IGARSS.2012.6350981.
- [11] He, K., Zhang, X., Ren, S., Sun, J., 2016. Deep residual learning for image recognition, in: CVPR.
- [12] Hou, B., Wang, Y., Liu, Q., 2017. Change detection based on deep features and low rank. IEEE Geoscience and Remote Sensing Letters 14, 2418–2422.
- [13] Kataoka, H., Shirakabe, S., Miyashita, Y., Nakamura, A., Iwata, K., Satoh, Y., 2016. Semantic change detection with hypermaps. arXiv preprint arXiv:1604.07513 2.
- [14] Li, X., Yuan, Z., Wang, Q., 2019a. Unsupervised deep noise modeling for hyperspectral image change detection. Remote Sensing 11, 258.
- [15] Li, Y., Peng, C., Chen, Y., Jiao, L., Zhou, L., Shang, R., 2019b. A

- deep learning method for change detection in synthetic aperture radar images. *IEEE Transactions on Geoscience and Remote Sensing* 57, 5751–5763.
- [16] Liu, S., Bruzzone, L., Bovolo, F., Zanetti, M., Du, P., 2015. Sequential spectral change vector analysis for iteratively discovering and detecting multiple changes in hyperspectral images. *IEEE transactions on geoscience and remote sensing* 53, 4363–4378.
 - [17] Liu, S., Du, Q., Tong, X., Samat, A., Bruzzone, L., 2019a. Unsupervised change detection in multispectral remote sensing images via spectral-spatial band expansion. *IEEE Journal of Selected Topics in Applied Earth Observations and Remote Sensing* 12, 3578–3587.
 - [18] Liu, S., Du, Q., Tong, X., Samat, A., Bruzzone, L., Bovolo, F., 2017a. Multiscale morphological compressed change vector analysis for unsupervised multiple change detection. *IEEE Journal of Selected Topics in Applied Earth Observations and Remote Sensing* 10, 4124–4137.
 - [19] Liu, S., Marinelli, D., Bruzzone, L., Bovolo, F., 2019b. A review of change detection in multitemporal hyperspectral images: Current techniques, applications, and challenges. *IEEE Geoscience and Remote Sensing Magazine* 7, 140–158.
 - [20] Liu, S., Tong, X., Bruzzone, L., Du, P., 2017b. A novel semisupervised framework for multiple change detection in hyperspectral images, in: 2017 IEEE International Geoscience and Remote Sensing Symposium (IGARSS), pp. 173–176.
 - [21] Long, J., Shelhamer, E., Darrell, T., 2015. Fully convolutional networks for semantic segmentation, in: CVPR.
 - [22] Lu, D., Mausel, P., Brondizio, E., Moran, E., 2004. Change detection techniques. *International Journal of Remote Sensing* 25, 2365–2401. URL: <https://doi.org/10.1080/0143116031000139863>, doi:10.1080/0143116031000139863, arXiv:<https://doi.org/10.1080/0143116031000139863>.
 - [23] Malila, W., 1980. Change vector analysis: An approach for detecting forest changes with landsat. *LARS Symposia*.
 - [24] Mou, L., Bruzzone, L., Zhu, X.X., 2018. Learning spectral-spatial-temporal features via a recurrent convolutional neural network for change detection in multispectral imagery. *IEEE Transactions on Geoscience and Remote Sensing* 57, 924–935.
 - [25] Mou, L., Hua, Y., Zhu, X.X., 2019. A relation-augmented fully convolutional network for semantic segmentation in aerial scenes, in: CVPR.
 - [26] Nam, H., Ha, J.W., Kim, J., 2017. Dual attention networks for multimodal reasoning and matching, in: CVPR.
 - [27] Nemmour, H., Chibani, Y., 2010. Support vector machines for automatic multi-class change detection in algerian capital using landsat tm imagery. *Journal of the Indian Society of Remote Sensing* 38, 585–591.
 - [28] Nielsen, A.A., 2007. The regularized iteratively reweighted mad method for change detection in multi- and hyperspectral data. *IEEE Transactions on Image Processing* 16, 463–478.
 - [29] Nielsen, A.A., Conradsen, K., Simpson, J.J., 1998. Multivariate alteration detection (mad) and maf postprocessing in multispectral, bitemporal image data: New approaches to change detection studies. *Remote Sensing of Environment* 64, 1 – 19. URL: <http://www.sciencedirect.com/science/article/pii/S0034425797001624>, doi:[https://doi.org/10.1016/S0034-4257\(97\)00162-4](https://doi.org/10.1016/S0034-4257(97)00162-4).
 - [30] Peng, D., Zhang, Y., Guan, H., 2019. End-to-end change detection for high resolution satellite images using improved unet++. *Remote Sensing* 11, 1382.
 - [31] Ronneberger, O., Fischer, P., Brox, T., 2015. U-net: Convolutional networks for biomedical image segmentation, in: *International Conference on Medical image computing and computer-assisted intervention*, Springer.
 - [32] Saha, S., Bovolo, F., Bruzzone, L., 2019. Unsupervised deep change vector analysis for multiple-change detection in VHR images. *IEEE Transactions on Geoscience and Remote Sensing* 57, 3677–3693.
 - [33] Simonyan, K., Zisserman, A., 2015. Very deep convolutional networks for large-scale image recognition, in: Bengio, Y., LeCun, Y. (Eds.), *3rd International Conference on Learning Representations*, ICLR 2015, San Diego, CA, USA, May 7–9, 2015, Conference Track Proceedings. URL: <http://arxiv.org/abs/1409.1556>.
 - [34] Singh, A., 1989. Review article digital change detection techniques using remotely-sensed data. *International Journal of Remote Sensing* 10, 989–1003. URL: <https://doi.org/10.1080/01431168908903939>, doi:10.1080/01431168908903939, arXiv:<https://doi.org/10.1080/01431168908903939>.
 - [35] Song, A., Choi, J., Han, Y., Kim, Y., 2018. Change detection in hyperspectral images using recurrent 3d fully convolutional networks. *Remote Sensing* 10, 1827.
 - [36] Volpi, M., Tuia, D., Camps-Valls, G., Kanevski, M.F., 2012. Unsupervised change detection with kernels. *IEEE Geoscience Remote Sensing Letter* 9, 1026–1030. URL: <https://doi.org/10.1109/LGRS.2012.2189092>, doi:10.1109/LGRS.2012.2189092.
 - [37] Wang, Q., Yuan, Z., Du, Q., Li, X., 2019. GETNET: A general end-to-end 2-D CNN framework for hyperspectral image change detection. *IEEE Transactions on Geoscience and Remote Sensing* 57, 3–13.
 - [38] Wang, X., Du, P., Chen, D., Liu, S., Zhang, W., Li, E., 2020. Change detection based on low-level to high-level features integration with limited samples. *IEEE Journal of Selected Topics in Applied Earth Observations and Remote Sensing* 13, 6260–6276. doi:10.1109/JSTARS.2020.3029460.
 - [39] Wang, X., Girshick, R., Gupta, A., He, K., 2018a. Non-local neural networks, in: *Proceedings of the IEEE conference on computer vision and pattern recognition*, pp. 7794–7803.
 - [40] Wang, X., Liu, S., Du, P., Liang, H., Xia, J., Li, Y., 2018b. Object-based change detection in urban areas from high spatial resolution images based on multiple features and ensemble learning. *Remote Sensing* 10. URL: <https://www.mdpi.com/2072-4292/10/2/276>, doi:10.3390/rs10020276.
 - [41] Yang, K., Xia, G.S., Liu, Z., Du, B., Yang, W., Pelillo, M., 2020. Asymmetric siamese networks for semantic change detection. arXiv preprint arXiv:2010.05687.
 - [42] Yang, M., Jiao, L., Liu, F., Hou, B., Yang, S., 2019. Transferred deep learning-based change detection in remote sensing images. *IEEE Transactions on Geoscience and Remote Sensing* 57, 6960–6973.
 - [43] Yuan, Z., Wang, Q., Li, X., 2018. Robust PCANet for hyperspectral image change detection, in: *IEEE International Geoscience and Remote Sensing Symposium (IGARSS)*.
 - [44] Zhan, Y., Fu, K., Yan, M., Sun, X., Wang, H., Qiu, X., 2017. Change detection based on deep siamese convolutional network for optical aerial images. *IEEE Geoscience and Remote Sensing Letters* 14, 1845–1849.
 - [45] Zhang, C., Yue, P., Tapete, D., Jiang, L., Shangguan, B., Huang, L., Liu, G., 2020a. A deeply supervised image fusion network for change detection in high resolution bi-temporal remote sensing images. *ISPRS Journal of Photogrammetry and Remote Sensing* 166, 183–200.
 - [46] Zhang, C., Yue, P., Tapete, D., Jiang, L., Shangguan, B., Huang, L., Liu, G., 2020b. A deeply supervised image fusion network for change detection in high resolution bi-temporal remote sensing images. *ISPRS Journal of Photogrammetry and Remote Sensing* 166, 183–200.
 - [47] Zhang, J., Lin, S., Ding, L., Bruzzone, L., 2020c. Multi-scale context aggregation for semantic segmentation of remote sensing images. *Remote Sensing* 12, 701.
 - [48] Zhang, W., Lu, X., 2019. The spectral-spatial joint learning for change detection in multispectral imagery. *Remote Sensing* 11, 240.
 - [49] Zhang, W., Lu, X., Li, X., 2018. A coarse-to-fine semi-supervised change detection for multispectral images. *IEEE Transactions on Geoscience and Remote Sensing* 56, 3587–3599.
 - [50] Zhao, W., Mou, L., Chen, J., Bo, Y., Emery, W.J., 2020. Incorporating metric learning and adversarial network for seasonal invariant change detection. *IEEE Transactions on Geoscience and Remote Sensing* 58, 2720–2731.